Towards custom built double core carbon nanothreads by stilbene and pseudo-stilbene type systems

Sebastiano Romi, Samuele Fanetti, Frederico Alabarse, Antonio Mio, Julien Haines, Roberto Bini

▶ **To cite this version:**

Sebastiano Romi, Samuele Fanetti, Frederico Alabarse, Antonio Mio, Julien Haines, et al.. Towards custom built double core carbon nanothreads by stilbene and pseudo-stilbene type systems. Nanoscale, 2022, 14 (12), pp.4614-4625. 10.1039/d1nr08188h . hal-03621782

HAL Id: hal-03621782
https://hal.umontpellier.fr/hal-03621782

Submitted on 30 May 2022

HAL is a multi-disciplinary open access archive for the deposit and dissemination of scientific research documents, whether they are published or not. The documents may come from teaching and research institutions in France or abroad, or from public or private research centers.

L'archive ouverte pluridisciplinaire **HAL**, est destinée au dépôt et à la diffusion de documents scientifiques de niveau recherche, publiés ou non, émanant des établissements d'enseignement et de recherche français ou étrangers, des laboratoires publics ou privés.

Towards Custom Built Double Core Carbon Nanothreads by Stilbene and Pseudo-Stilbene Type Systems

Sebastiano Romi,[†] Samuele Fanetti,[*,‡,†] Frederico Alabarse,[¶] Antonio M. Mio,[§] Julien Haines,[‖] and Roberto Bini[*,⊥,†,‡]

[†]*LENS, European Laboratory for Non-linear Spectroscopy, Via N. Carrara 1, I-50019 Sesto Fiorentino, Firenze, Italy*

[‡]*ICCOM-CNR, Istituto di Chimica dei Composti OrganoMetallici, Via Madonna del Piano 10, I-50019 Sesto Fiorentino, Firenze, Italy*

[¶]*ELETTRA, Elettra Sincrotrone Trieste S.C.p.A, in AREA Science Park 34149 Basovizza, Trieste, Italy*

[§]*IMM-CNR, Istituto per la Microelettronica e Microsistemi, VIII Strada 5 - Zona Industriale 95121 Catania, Italy*

[‖]*Institut Charles Gerhardt Montpellier - UMR 5253 CC1504 Place Eugène Bataillon Bât. 15 - 34095 Montpellier, France*

[⊥]*Dipartimento di Chimica "Ugo Schiff", Università di Firenze, Via della Lastruccia 3, I-50019 Sesto Fiorentino, Italy*

E-mail: fanetti@lens.unifi.it; roberto.bini@unifi.it

Phone: +390554572436; +390554572489

Abstract

Until recently, saturated carbon nanothreads were the missing tile in the world of low-dimension carbon nanomaterials. These one-dimensional fully saturated polymers possess superior mechanical properties by combining high tensile strength with flexibility and resilience. They can be obtained by compressing above 15 GPa aromatic and heteroaromatic crystals exploiting the anisotropic stress that can be achieved by the diamond anvil cell technique. Recently, double-core nanothreads were synthesized by compressing azobenzene crystals achieving the remarkable result of preserving untouched the azo group as a linker of the resulting double thread. Herein, we demonstrate the generality of these findings through the synthesis of double carbon nanothreads from trans stilbene and azobenzene-stilbene mixed crystals. Employment of Fourier Transform Infrared Spectroscopy and synchrotron X-ray diffraction allowed to characterize the reactivity identifying reaction threshold, kinetics and structure-reaction relationship. In particular, the reaction is anticipated by a phase transition characterized by a sudden increase of the monoclinic angle and a collapse along the b axis direction. Large bidimensional crystalline areas extending several tens of nanometers are evidenced by Transmission Electron Microscopy also confirming the monoclinic unit cell derived by X-ray diffraction data in which thread possessing the polymer 1 structure, as suggested by Density Functional Theory calculations, are packed. The most exciting result of this study is the demonstration of viable synthesis of double nanothreads where the number and the nature of cromophoric groups linking the threads can be dosed by preparing starting crystals of desired composition thanks to the isomorphism proper of the pseudo-stilbene molecules. This is extremely important in tailoring nanothreads with tunable optical properties and adjustable band gap also exploiting the possibility of introducing substituent in the phenyl groups.

The number and the applications of pure or hybrid carbon nanomaterials impressively grew in the last years encompassing many different research areas like energy storage, biomedical and environmental applications, organic solar cells, sensors and biosensors, imaging, material science and many others.[1–3] These applications mainly regards the use of pure or composite materials based on graphene,[4] nanotubes[5,6] and nanodiamonds.[7] Among pure carbon nanomaterials, saturated carbon nanothreads are the last discovered filling the gap concerning the existence of fully sp^3 carbon 1D diamond-like chains. These materials are expected to be characterized by extraordinary mechanical properties combining a stiffness only slightly less than diamond, with flexibility, resilience and excellent tensile strength.[8] Saturated carbon nanothreads were predicted[9–11] well in advance with respect to the first reported synthesis realized by compressing benzene in a diamond anvil cell (DAC).[12] After this first achievement the number of syntheses and the comprehension of reaction mechanisms impressively grew thus putting the basis for potential technological applications.[13,14] Nanothreads were indeed produced by compressing different aromatics like pyridine,[15,16] aniline,[17] thiophene,[18] furan,[19] arene-perfluoroarene co-crystals,[20,21] but also fully saturated strained molecules like cubane.[22] This number further increases when computational studies are taken into account, since fully saturated carbon nanothreads have been reported from polycyclic aromatic hydrocarbons[23] and substituted benzenes (-CH_3, -NH_2, -OH, -F).[24] As far as the mechanism is concerned, the nanothreads formation is often non topochemical mostly benefiting of the uniaxial stress intrinsic to the use of the DAC while avoiding any hydrostatic compression medium.[25,26] Consequently, the competition between topochemical and stress driven reactivity limits the nanothread yield and the exploitation of temperature to improve the quality and to increase the reaction yield.[16,27] The reaction mechanism reflects in the nanothreads' structure which exhibit a relative parallel arrangement forming pseudohexagonal 2D lattice domains with a correlation length of tens of nm but definitely much shorter ($\leq$ 2.5 nm) along the threads.[28,29] This is due to the presence of unsaturations and defects which rule the quality and length of the threads,[8,30] but, on the other hand, can

also be used for tuning the electronic properties.[31] Designing and tailoring nanothreads with customized features is presently the main challenge from experimental point of view and its realization goes through the knowledge of the structure-reaction relationships of the starting crystal and the control of number and types of unsaturations or substituent groups. In fact, the presence of heteroatoms or substituents outside of the thread backbone can be readily available as potential linkers or active sites for doping, besides concurring to determine the electronic properties of the nanothread, without altering its mechanical characteristics.[31]

Recently, a double nanothread linked by untouched azo groups was synthesized by compressing azobenzene above 20 GPa.[32] X-ray diffraction studies suggest a polymerization process involving equivalent molecules stacked along the b axis[33] and leading to the formation of high quality double core nanothreads presenting a polymer-1 geometry. The nanothreads obtained are arranged in large bundles having a pseudohexagonal 2D ordered structure with a distance between the planes, identified by the centres of the threads, of 5.6 Å. However, the most relevant result concerns the preservation of the azo group, an occurrence having a twofold importance. The first one is related to the photophysical and photochemical properties of azobenzenes which represent a versatile class of dyes and thanks to the efficient photoisomerization are employed for the realization of molecular devices, functional and composite materials.[34–38] The second aspect is represented by the close similarities of azobenzene with the pseudo stilbene class of molecules, being characterized by a similar molecular structure, where only the linking group changes (for example ethyl, ethenyl, ethynyl), and presenting an isostructural crystal packing making possible the formation of substitutionally mixed crystals.[39–41] The composition of the starting crystal can be therefore adjusted, by changing for example the relative concentration of the pseudo stilbene molecules or introducing ring substituents, for tuning the optical and electronic properties of the synthesized material.

The ambient pressure crystal structures of t-azobenzene (TA) and t-stilbene (TS) are monoclinic, $P2_1/c$, with two molecules in the asymmetric unit cell[39,40] located at inversion centers and with one of them characterized by dynamic orientational disorder.[42] The TA

structure has also been characterized up to 12 GPa using nitrogen as pressure transmitting medium.[33] The $P2_1/c$ structure holds up to about 9.5 GPa where a phase transition is observed likely related to a structural adjustment precursor of the nanothread formation. In addition to be isostructural and exhibiting the same kind and degree of disorder, TA and TS are also characterized by almost identical packing coefficient thus making possible the formation of mixed crystals with continuously adjustable relative concentration. Mixed crystals having four different compositions (from TS:TA $\sim$ 2:1 to TS:TA $\sim$ 1:3) were structurally characterized at ambient pressure by X-ray and neutron diffraction.[41] Besides confirming the perfect miscibility and the retention of the crystal structure, this study pointed out that stilbene molecules preferentially occupy the disordered site, which presents more available volume, and that the evolution of the lattice parameters with the composition nicely fit the Vegard's law therefore indicating a perfect substitution without volume excess.

Here we show the formation of double nanothreads by compressing TS and 1:1 TS-TA mixed crystals. The reaction has been characterized by Fourier Transform Infrared Spectroscopy (FTIR) and the crystal evolution monitored by X-ray diffraction (XRD). An extensive characterization of the nanothreads has been achieved by XRD, FTIR and Transmission Electron Microscopy (TEM) and further supported by density functional theory (DFT) calculations. Different pressure and temperature conditions have also been followed to identify where the quality and the yield of double nanothreads are maximized. This is the first attempt to synthesize a fully saturated carbon nanothread controlling the concentration of specific chromophores a prerequisite for achieving an efficient tuning of the optical properties.

Results and Discussion

The pressure evolution of different pure TS and TS-TA mixed crystals was monitored at ambient temperature by using both FTIR spectroscopy and synchrotron XRD up to pressures exceeding 30 GPa. In all the cases a reaction was observed and in some experiments we also

characterized the kinetics. High-temperature (up to 430 K) isothermal compression experiments were also performed in the attempt of discovering the optimal reaction conditions in terms of yield and product quality. In view of the large number of samples investigated, we will present the results separating the different aspects of the characterization and, within each of them, presenting separately the results for pure TS and TS-TA mixed crystals.

Characterization of the reaction by FTIR spectroscopy

Stilbene

Polycrystalline TS stilbene samples were compressed without pressure transmitting medium (PTM) at ambient temperature and at 375 K. As already reported in the case of TA, [32] some subtle spectral changes occur between 7 and 10 GPa where a phase transition was evidenced by XRD in TA. [33] The monomer band progressively broaden and weaken with rising pressure (see Figure 1) vanishing at about 30 GPa.

The onset of the reaction slightly changes depending on the waiting time between two consecutive spectra (see Figure 2), sample and compression rate, but in all the ambient temperature studies ranges between 16 and 20 GPa. The reaction's onset cannot be directly identified by the spectral changes because of the broadness of the monomer and product bands at high pressure and by the sluggishness of the transformation. However, comparison of subsequent spectra acquired at the same, or very close, pressure values, allows for the precise onset's identification. In Figure 2 we report the difference spectrum obtained by the subtraction of two spectra registered at the same pressure, 19.8 GPa, but separated by about 15 hours. The sharp negative peaks in the difference spectrum remark the reduction of the monomer amount whereas the much broader positive peak just below 3000 cm^{-1} is due to the saturated carbon atoms which characterize the product. The sensitivity of the method should be remarked, since the intensity variations are in the order of hundredth of absorbance units. Compression at higher temperature entails a significant decrease of the threshold pressure as observed in aniline, [27] pyridine[16] and also azobenzene. [32] In Figure 3

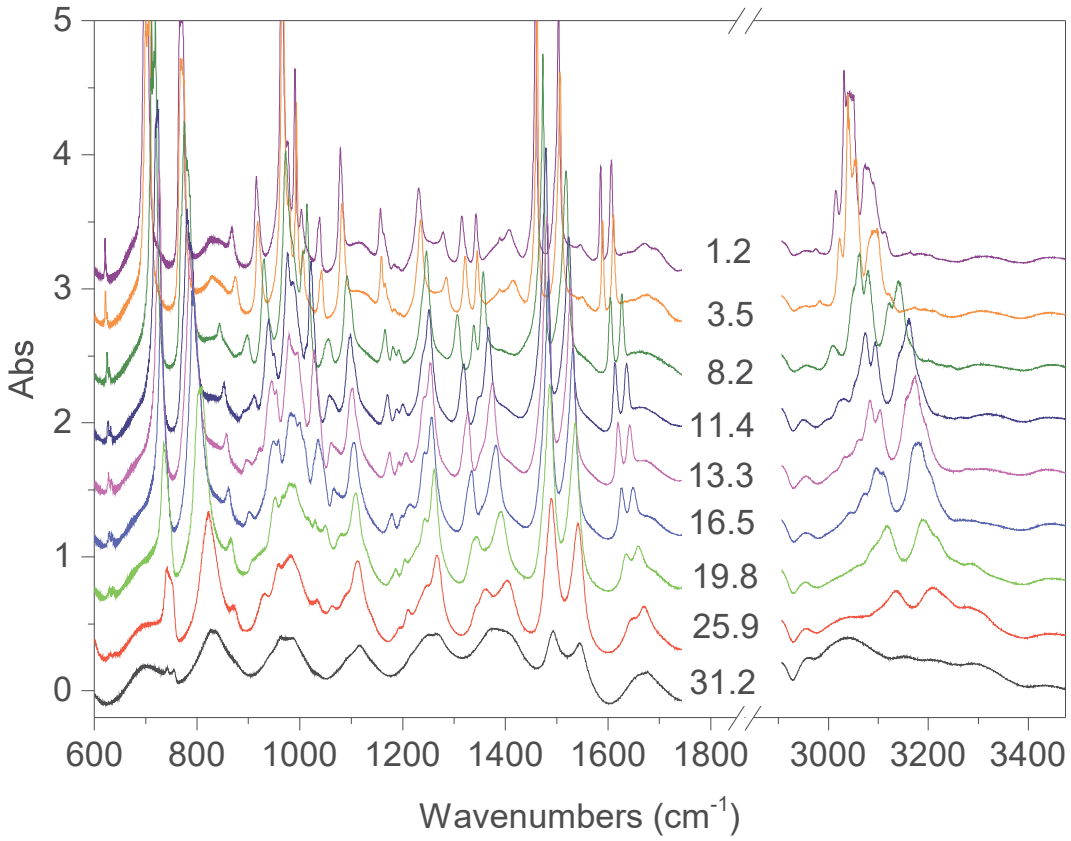

Figure 1: Representative spectra showing the evolution of the IR absorption spectrum of TS crystal on increasing pressure at ambient temperature. The pressure values reported are expressed in GPa.

we report some IR absorption spectra measured during an isothermal compression at 373 K. The sample was first compressed at ambient temperature up to 10 GPa, thus well below the reaction's onset, and then isobarically heated to 373 K and then compressed again. In this case the signatures of the chemical transformation were observed at 14.5 GPa.

The transformation rate at the reaction's onset is extremely slow therefore, once the latter was identified, the samples were rapidly (2-4 minutes) compressed few GPa above to study the kinetics. To this purpose we measured the absorbance decrease of selected intense TS bands presenting a reduced width and not overlapping with other monomer or product absorptions. These requirements are satisfied by the strong doublet characterizing the spectrum around 1500 cm^{-1} (1460 and 1503 cm^{-1} at 1.2 GPa; 1495 and 1549 cm^{-1} at

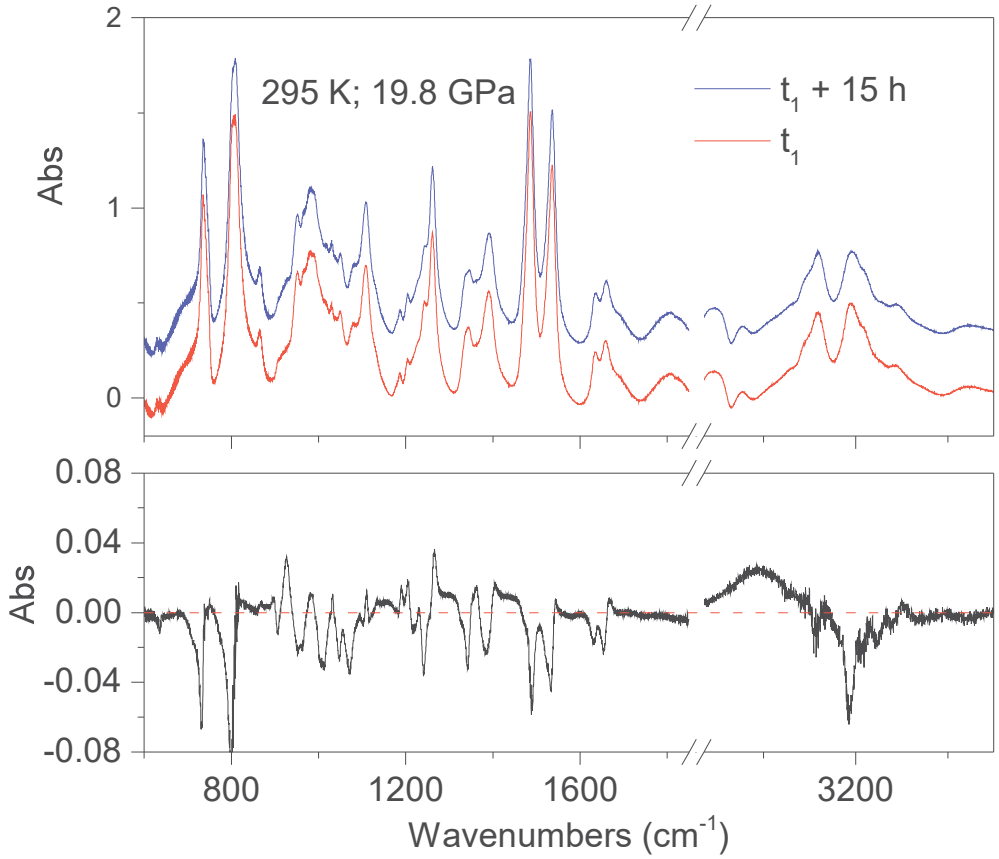

Figure 2: Difference spectrum (lower panel) obtained by subtracting the two spectra (upper panel) collected at ambient temperature and nearly the same pressure (19.8 GPa) 15 hours apart. Negative and broad positive peaks are related to disappearing and forming species, respectively.

24 GPa) assigned to ring stretching modes.[43] The time evolution of the absorbance of these bands was reproduced by using the Avrami model originally developed to describe the crystal growth from the melt[44–46] and then extended to the study of diffusion controlled solid-state reactions.[47] By indicating with $R(t) = [I(0) - I(t)]/I(0)$ the fraction of TS monomer reacted as a function of time, where the intensity I is relative to the selected TS bands, the fitting relation is given by:

$$R(t) = R_\infty \left[1 - e^{[-k(t-t_0)^n]}\right] \tag{1}$$

The fit parameters are R_∞, corresponding to $[I(0) - I(\infty)]/I(0)$, the reaction starting time

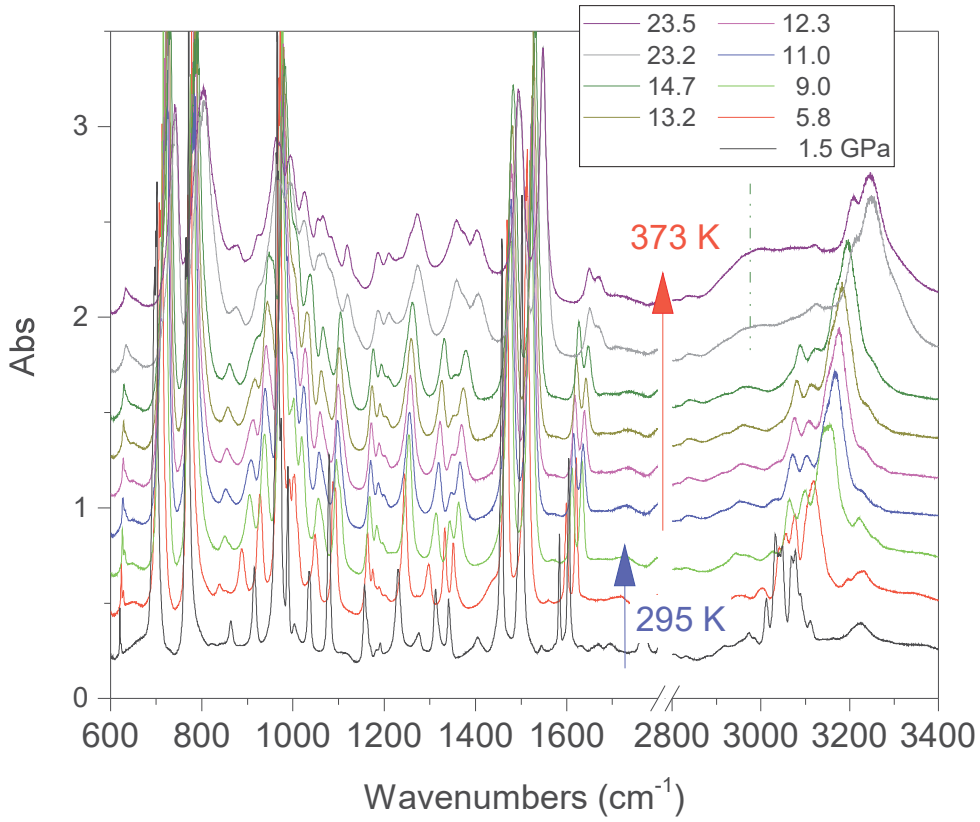

Figure 3: Evolution of the IR spectra of crystalline TS along a high temperature compression. The sample has been compressed at ambient temperature up to 9 GPa, heated at this pressure up to 373 K and then isothermally compressed. The reaction threshold has been identified around 14 GPa. The broken line identifies the position of the broad C-H stretching band involving saturated carbon atoms.

t_0, the rate constant $k^{1/n}$ and n which is related to the dimensionality of the growth process. In Figure 4 we report the time evolution of the $R(t)$ data as obtained by the fit of the ring stretching absorption bands at about 1500 cm^{-1} in two different experiments where the kinetics was studied at comparable pressure values but different temperatures: ambient (upper panel) and 373 K (middle panel). As it can be seen by the values of the fitting parameters, reported as insets, we have a very reproducible behavior in the two cases with almost 30% of reacted monomer, a very similar rate constant and the same n value which attests for a unidimensional growth of the reaction product. A very interesting element to

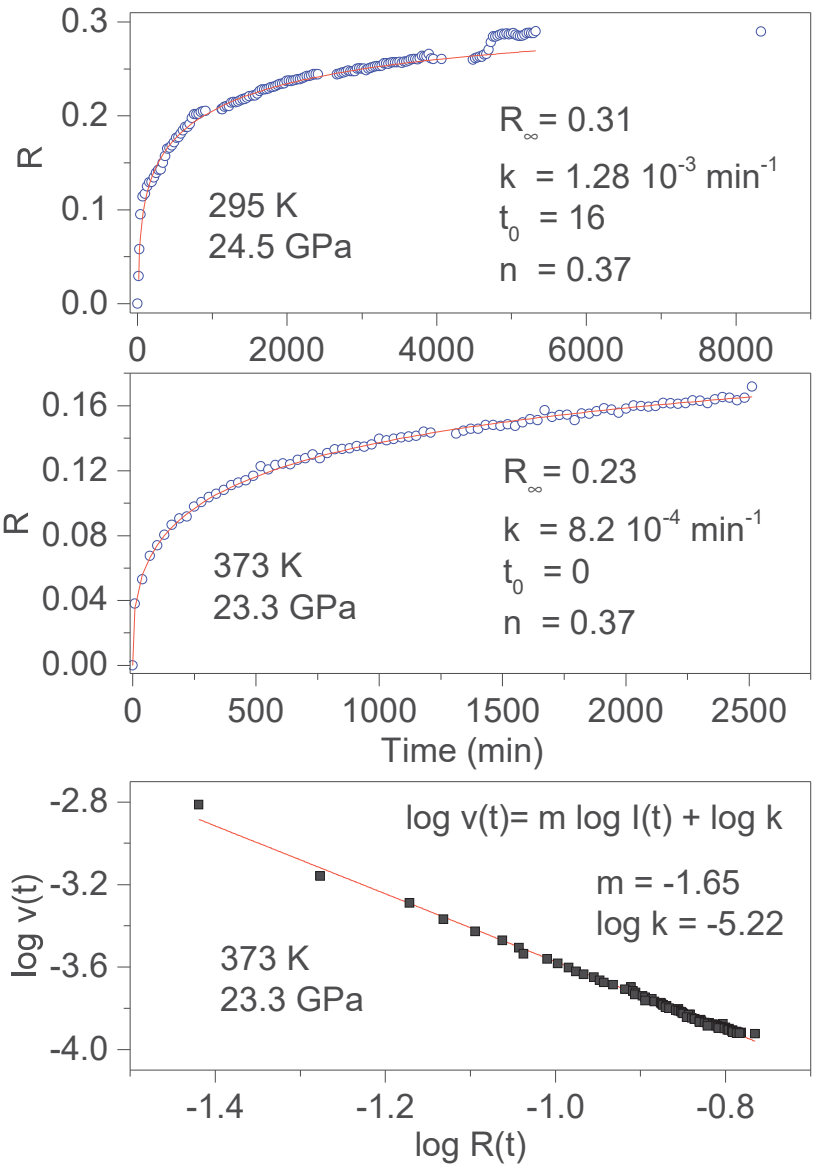

Figure 4: Kinetics of the reactions performed at ambient temperature and 24.5 GPa (upper panel) and at 373 K and 23.3 GPa (middle panel) in pure TS. The fraction of monomer reacted, determined by the absorption of selected stilbene bands (see text), is plotted as a function of time. The red lines in these two panels are the fit of the experimental data using Avrami's law (eq.1), the fitting parameters are reported in both cases as an inset. The clear step after about 5000 hours in the room temperature reaction is related to photochemical effects caused by the laser employed to excite the ruby fluorescence. In the lower panel the log-log plot from which the molecularity of the process, the slope value of the linear evolution, is determined (see text).

be discussed is represented by the small step clearly visible in the data evolution reported in the upper panel after about 5000 minutes. This occurrence is directly related to an insisted

search of the ruby for checking the sample pressure. In spite of using only 1 mW of 532 nm cw laser emission, a clear sudden increase of the amount of reacted monomer occurred thus indicating a photoinduced reactivity whose origin is however difficult to ascribe to the reaction with other monomers or with the reaction product.

Further insight about the reaction mechanism can be derived by the analysis of the molecularity of the process. To this purpose we adopted a simple kinetic relation where the reaction rate v is assumed proportional to the monomer concentration $[M]$ through the rate constant k and the process' molecularity m: $v = k\,[M]^m$.[48] The analysis is performed using the log-log form $log\ v(t) = m\ log\,[M] + log\ k$. In order to calculate the value of the reaction rate along the entire transformation process, we reproduced by a stretched exponential the time evolution of the monomer concentration, i.e. the absorbance value of the selected monomer bands, so as to have an analytical function to derive. In the lower panel of Figure 4 the log-log plot is reported for the high temperature reaction. The data are nicely reproduced by a single straight line with a slope value, the molecularity, of 1.65 consistent with a rate limiting step involving two molecules and with a linear accretion of the product.

Mixed crystal

The formation of substitutional TS-TA mixed crystals was checked by FTIR spectroscopy before their loading in the DAC (S1). The behavior of the TS-TA mixed crystals under compression is identical to the one observed for pure TS. Also in this case the IR absorption spectra (S1) provide evidence for a chemical reaction with onset at about 20 GPa and a very slow transformation rate which can be increased only by further compression between 25 and 30 GPa. As discussed in the case of TS, we also tested the reactivity at temperatures higher than ambient. A mixed TS-TA crystalline sample was first compressed up to 8.9 GPa and then heated at 373 K. At this temperature it was isothermally compressed up to 24.1 GPa, pressure where the kinetics was investigated through the analysis of the absorbance

evolution as a function of time of the peaks falling between 700 and 850 cm^{-1} (see Figure 5). In spite of the apparent complexity of this region, product bands growing in between the monomer peaks can be easily identified, thus obtaining from the spectral deconvolution the data relative to both the monomer consumption and the product formation. In Figure 5 we also show the time evolution of both monomer and product fractions as obtained by summing the area of all monomer and product bands, respectively. The two kinetic curves can be reproduced by the Avrami law (see eq. 1) using the same fitting parameters. This is a crucial information supporting the occurrence of a selective reaction leading, as we will see, to the formation of saturated carbon nanothreads. Finally, in the last panel of Figure 5 we report the total area of the product band vs reaction time and the relative fit performed by using the Avrami's law. In this case the relation is written as:

$$A(t) = A_{\infty} e^{[-k(t-t_0)^n]} \tag{2}$$

where A_{∞} is the absorbance value at the equilibrium whereas the other three parameters t_0, $k^{1/n}$ and n have been previously defined. Remarkably, the rate constant and the n parameters are exactly the same of those employed to reproduce the kinetics of pure TS at nearly the same P-T conditions (see Figure 4) by using the monomer consumption as a function of time.

X-ray diffraction

An angle dispersive X-ray diffraction (ADXRD) synchrotron study, recently carried out as a function of pressure on the parent TA crystal, disclosed the structure-reaction relationship identifying the direction along which the molecules interact to form the double core carbon nanothreads.[33] The reaction is anticipated by a reversible phase transition occurring around 9.5 GPa when the TA powder is quasi-hydrostatically compressed, and at slightly lower pressure, ~7 GPa, when no pressure transmitting medium is employed. This transition

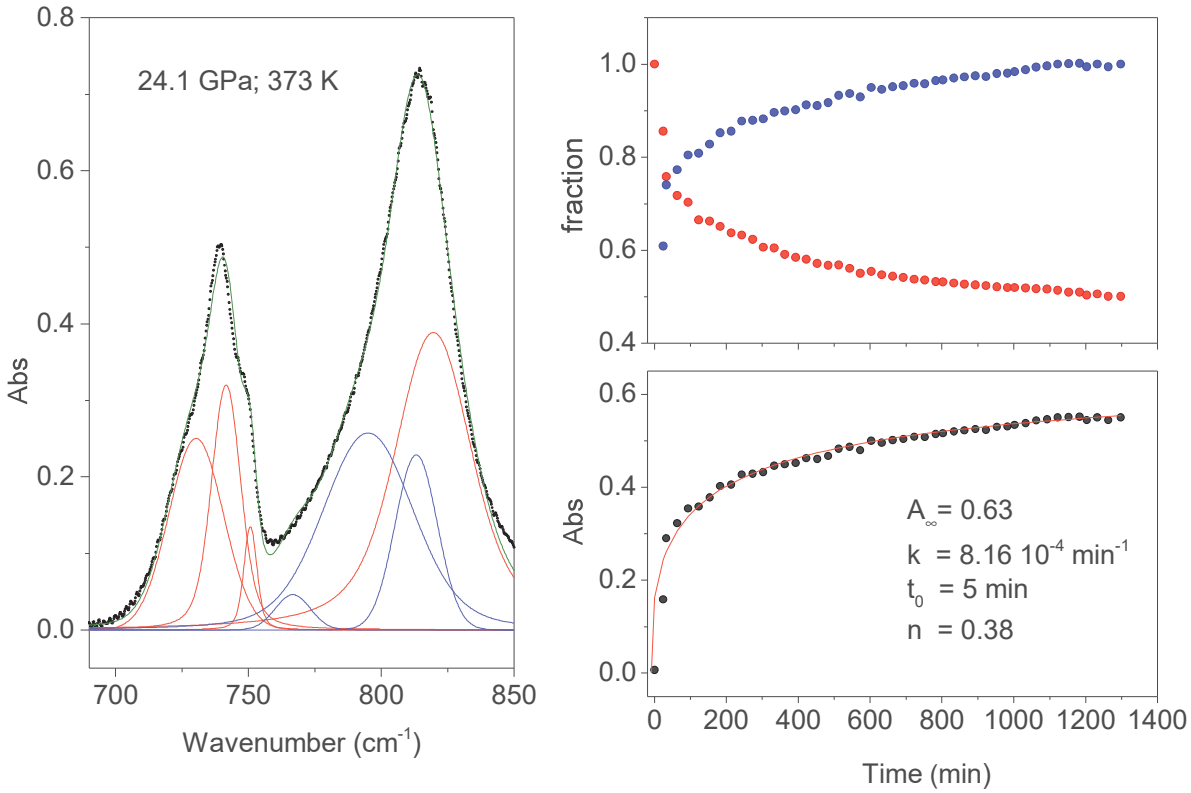

Figure 5: Left: example of deconvolution of the spectral region employed for following the kinetics of the transformation of the mixed TS-TA crystal at 24.1 GPa, red and blue bands belong to the monomer and to the product, respectively. Right: in the upper panel the comparison of the time evolution of the fractional total absorbance $A(t)/A(0)$ for the monomer as red dots, $A(t)/A(\infty)$ for the product as blue dots is shown. The $A(t)$ values are obtained by summing the area of all the bands of the monomer (red) or of the product (blue). In the lower panel we report the fit by the Avrami's law of the total absorbance of the product bands considered.

consists of a sudden increase of 5-6 degrees of the monoclinic angle and a decrease of the b length, changes leading to a volume reduction of about 12%. After the transition all the cell parameters remain practically unchanged with the exception of the b length that shortens of a further ~7% up to 19 GPa. As a consequence, the distance among nearly parallel phenyl rings along the b axis is estimated, once the phonon dynamics is taken into account,[27,49,50] to be 2.5 Å around 19-20 GPa pressure where we locate the reaction onset, a distance short enough to allow the formation of inter-ring C-C σ-bonds. The b axis is therefore identified

as preferential axis for the reaction propagation, thus becoming the nanothreads axis.

According to the isomorphism existing among the pseudo-stilbenes class crystals, a similar behavior is expected also for TS and TS-TA mixed crystals. In Figures 6 and 7 we report the integrated patterns of pure TS and TS-TA mixed samples compressed without pressure transmitting medium. In both cases it is evident, as already observed for pure TA, [33] a rapid deterioration of the pattern quality between 6 and 10 GPa, and the correlation existing between the higher angle diffraction peak of the product, one of the two observable after decompression, and specific reflections of the monomeric crystal. In addition, the lowest 2θ reflection of the product is already visible, especially in the TS-TA mixed crystal, far below the reaction onset, which is precisely located by the FTIR absorption measurements, thus evidencing the close relation between the molecular arrangement in the pristine crystals and in the nanothread.

As reported in S2, the patterns could be successfully and completely assigned using the monoclinic $P2_1/c$ structure proper of both TS [39,40] and TS-TA mixed crystal. [41] Accordingly, we determined the lattice parameters and the volume at each pressure value, and their evolution with pressure is reported in Figure 8 and compared to that relative to pure TA crystal data. [33] A sudden jump of the monoclinic angle, about 5 degrees, occurs between 9 and 10 GPa, and also the volume has a discontinuity in the same pressure range. Both features are particularly evident in the TS crystal. Above this pressure all the parameters are nearly constant with the exception of the b axis which instead undergoes to a remarkable reduction, especially in the case of mixed TS-TA crystal, which appears as the only cause of the further volume decrease. All these features are common to all the investigated TA, TS and mixed crystals.

Recovered materials

The materials synthesized in the different experiments have been recovered at ambient conditions and characterized by FTIR spectroscopy, XRD and high-resolution TEM. We also

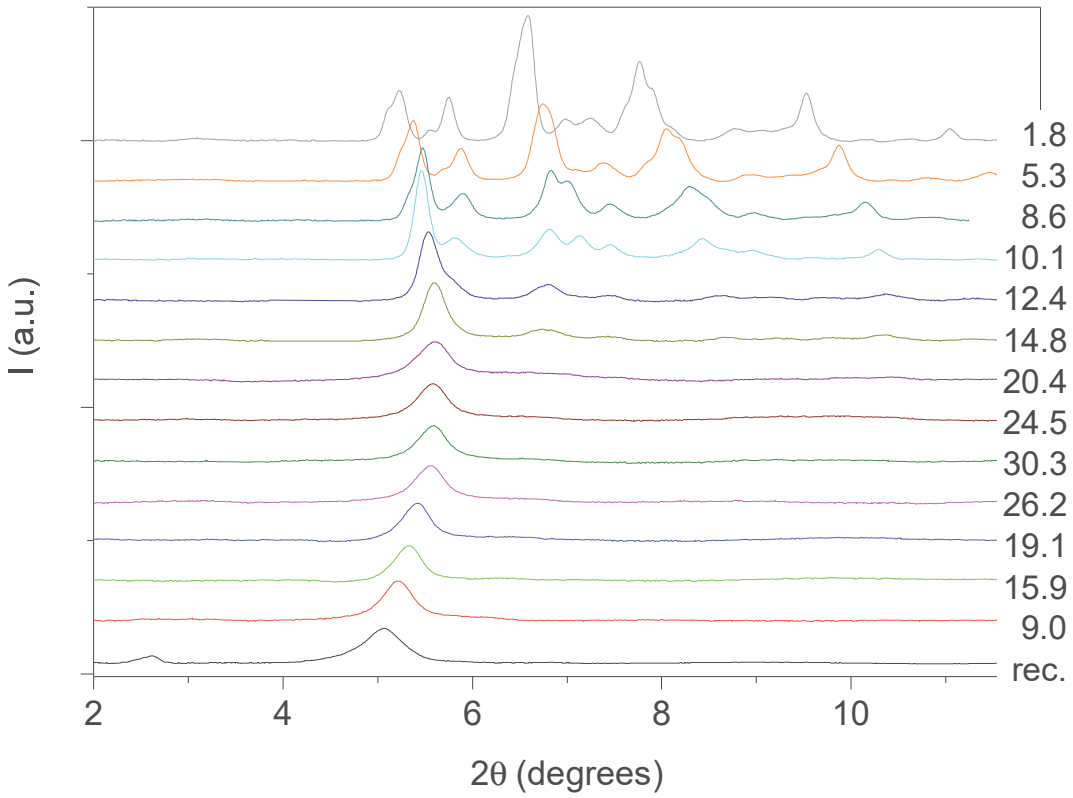

Figure 6: Selected X-ray diffraction patterns collected ($\lambda = 0.49499$ Å) on pure TS during a room temperature compression-decompression cycle performed without pressure transmitting medium. The pressure values reported for each pattern are in GPa.

attempted to measure Raman spectra but the huge fluorescence background and the sudden damage of the sample even using few mW at 660 nm prevented this characterization. Once the decompression was completed, FTIR spectra were measured before and after the cell opening, and after keeping in vacuum for several hours the recovered material to remove a consistent amount of the residual monomer. FTIR spectroscopy was also used to test over time the chemical stability of the recovered materials which was found unaltered after several weeks the opening of the cell. In Figure 9 we report the IR absorption spectra of representative TS and TS-TA samples recovered from both room and high temperature experiments. As expected from the only partial transformation of the starting crystal during

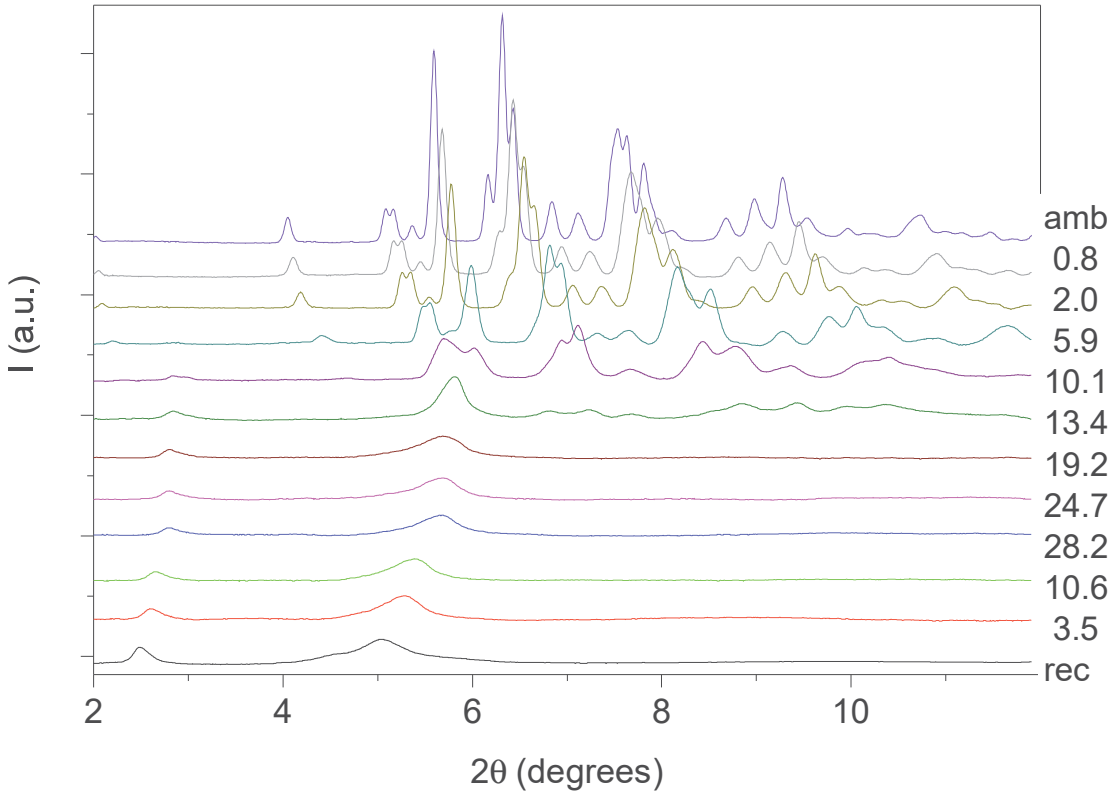

Figure 7: Selected X-ray diffraction integrated patterns collected (λ = 0.49499 Å) on a TS-TA mixed crystalline powder during a room temperature compression-decompression cycle performed without pressure transmitting medium. The pressure values reported for each pattern are in GPa.

the reaction, about 30%, monomer bands are observed in the quenched material. This is clearly visible in the left panel of Figure 9 by comparing the black and red trace which are relative to the same sample recovered at ambient conditions but registered before an after opening the cell and pumping over the sample for several hours thus allowing the monomer removal. Interestingly, a new band appears in many samples after the cell opening at 1730 cm^{-1}, a feature that can be assigned to the formation of a very small amount of carbonyl terminations. The spectral similarities among the materials recovered from the transformation of pure TS, TA and TS-TA mixed crystals clearly indicate common bonding characteristics and hybridization of the carbon atoms pointing to the successful synthesis of double-core

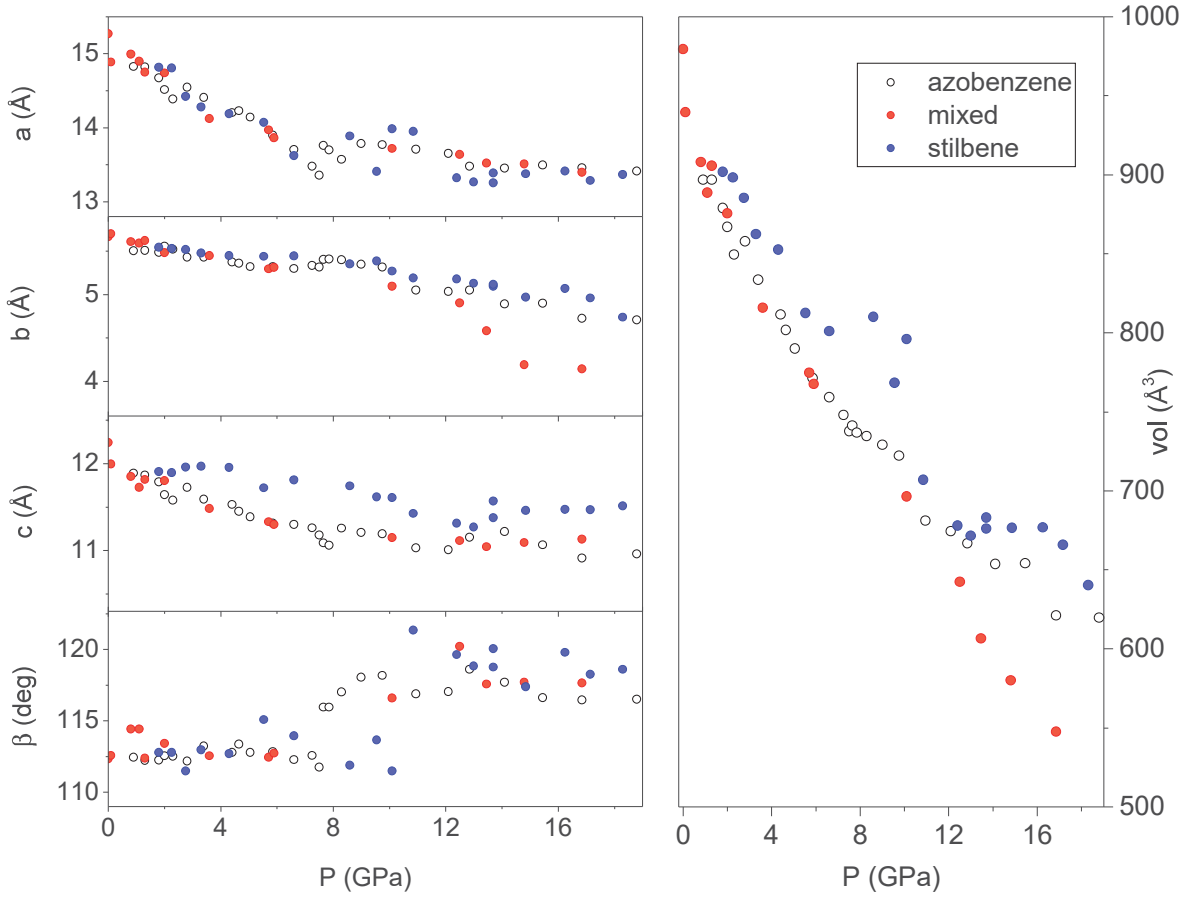

Figure 8: Pressure evolution of the lattice parameters as derived by Le Bail refinement of the XRD integrated patterns of TA, TS and TS-TA mixed crystals all compressed without pressure transmitting medium. The data for TA crystal are from ref.[33] The pressure values reported for each pattern are in GPa.

carbon nanothreads. Peculiar differences are represented by the strong intensity of the high frequency doublet (1495 and 1600 cm^{-1}) in the products from TS-TA mixed crystals observed also in pure TA and deriving from the contribution of the N=N stretching mode connecting the double nanothreads,[32] and by the peak just above 960 cm^{-1} clearly visible in the product of TS (marked by hashes) and slightly weaker in that from mixed TS-TA crystals. This band is characteristic of CH wagging mode of *trans*-dialkyl ethylene groups,[51] thus providing evidence of the ethylenic group preservation in the final product in perfect agreement to that observed in azobenzene.[32]

The formation of double-core carbon nanothreads linked by ethylenic and azo groups

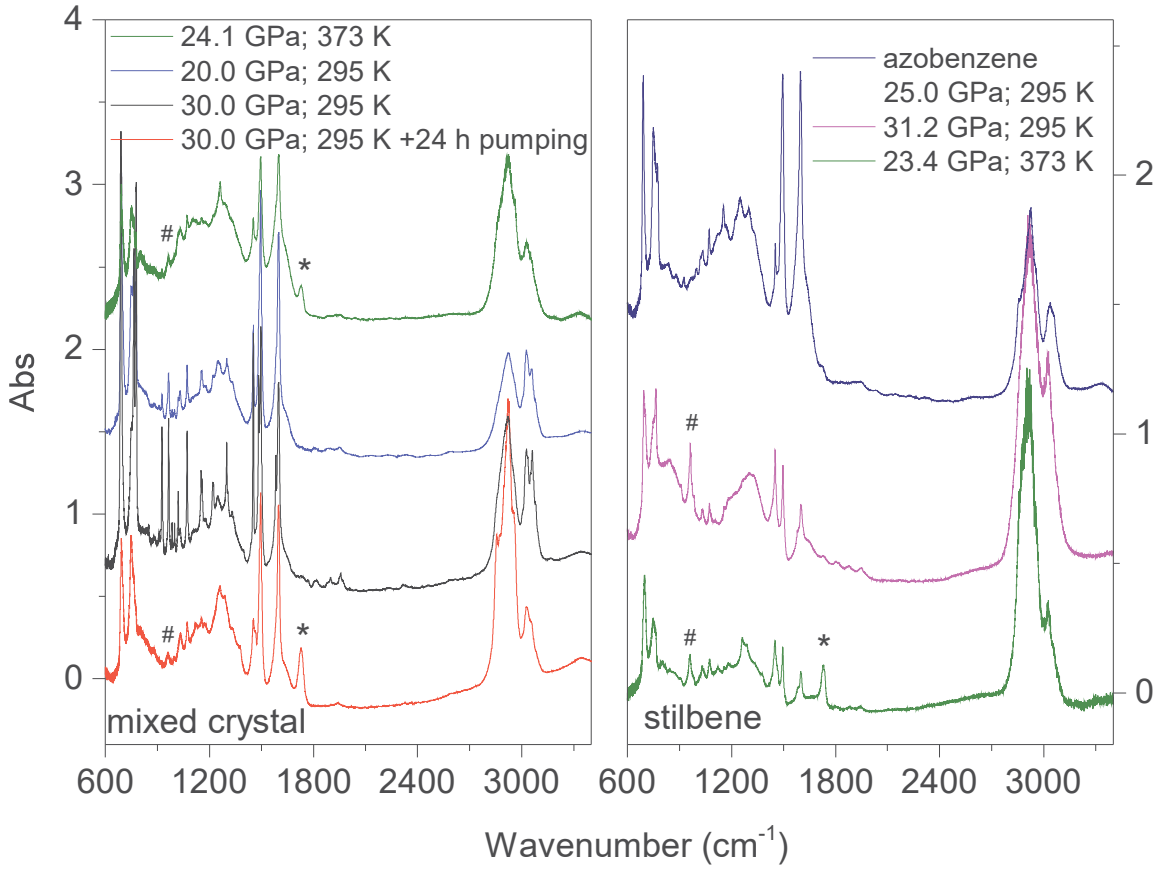

Figure 9: IR absorption spectra of some products recovered at ambient conditions after being removed from the diamonds. The reaction conditions are reported in the insets. Left: products spectra of the mixed crystals transformation at three different pressures, the residual monomer peaks are easily identified by the comparison of the product's spectra from the reaction at 30 GPa measured immediately after opening the cell (black trace) and after further 24 hours kept in vacuum (red trace). Right: products' spectra relative to the compression of stilbene crystals at two different pressures and temperatures, both spectra have been measured after the samples were kept several hours in vacuum. For comparison a typical spectrum of the material recovered from the analogous azobenzene transformation is also reported. The bands labeled by asterisks form during the cell opening and are assigned to carbonyl terminations whereas the ones marked by ashes indicate CH wagging characteristic of trans-dialkyl ethylene groups.

is also supported by the ADXRD patterns of the samples quenched at ambient conditions. The spotty nearly hexagonal XRD pattern, always taken as an evidence of the 2D ordered packing in the plane perpendicular to the nanothread axis,[15,16,26,32] characterizes many of the recovered products. Some of these patterns are reported in Figure 10. They are fully compatible with those obtained in pure TA where the double nanothreads were arranged

in a distorted pseudo-hexagonal 2D lattice with axes of 13.05 and 6.45 Å, and forming an angle very close to 120°.[32,33] This structure was identified by three diffraction peaks, (001), (10-1) and (100) axis choice as in ref.,[33] whose position in the pure TA case is also indicated by dashed lines in Figure 10. From the comparison of the different recovered materials an appreciable dispersion of the peaks position is observed, varying from 5.6 to 6.0 and from 10.8 to 11.4 Å for the (001) and (100) reflections, respectively. As already reported in the TA case, the width of the (001) and (10-1) reflections are narrower than (100) which, on turn, is often asymmetric or even split. All these features are likely related to the presence of some type of disorder in the 2D arrangement particularly pronounced along the longer axis, however they cannot be rationalized on the basis of the P-T conditions of the synthesis and are suggestive of a greater complexity ruling the nanothreads packing. It is also important to recall that the beam dimension used (∼80 and ∼150 μm for the experiments conducted at Xpress and in-house, respectively) probes almost the entire sample thus providing and average information about the structural properties of the sample. As shown in Figure 10 not all the recovered materials present a hexagonal spotty patterns being in many cases characterized by homogeneous diffraction rings indicating a powdered sample showing no evidences of preferred orientations. This occurrence is strictly related to the pressure of the synthesis and to the characteristics of starting samples: lower the pressure and larger the monomer crystallites, better defined hexagonal spotty patterns are obtained. On the contrary, when the sample was finely grinded, as in the case of the two TS-TA mixed crystals reported in Figure 10, perfect homogeneous rings were obtained.

We also checked the effect of thermal annealing on the structural characteristics of the recovered material by heating in vacuum to 433 K the product of the reaction performed at 23.4 GPa and 373 K in pure TS (st3 in Figure 10). The sample was kept for approximately one hour at the annealing temperature while we monitored the IR spectrum to check possible chemical changes that were not detected. The ADXRD pattern measured once the ambient temperature was recovered (S2) did not show significant changes in the lineshape of the

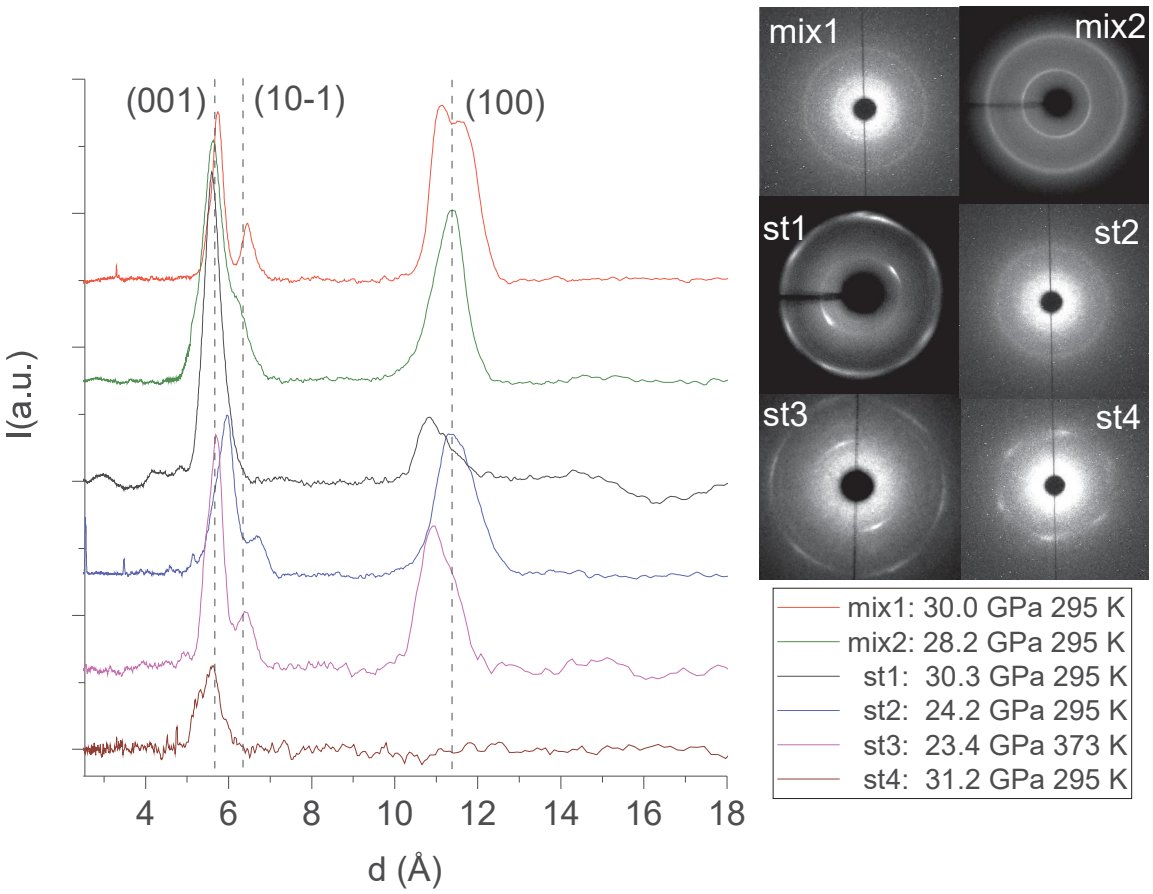

Figure 10: 1D azimuthally integrated diffraction patterns reported as a function of the d spacing of the materials recovered at ambient conditions by different experiments with both pure TS and TS-TA mixed crystals. On the right side the corresponding 2D images are also reported. Samples mix2 and st1 have been acquired with synchrotron light whereas all the remaining patterns have been recorded with the in-house set-up. The baseline of integrated patterns has been obtained by subtracting the Compton background. The three dashed lines indicate the position of the (001), (10-1) and (100) diffraction peaks of the distorted pseudo-hexagonal 2D monoclinic cell in which the azobenzene nanothreads are arranged.[32,33]

different peaks indicating that no substantial improvement of the threads and of the lattice quality is achieved. On the other hand, a consistent increase of the d spacings (0.2-0.3 Å) takes place likely ascribable to relaxation of the residual stress inherent to the compression-decompression cycle and to the chemical transformation.

A better definition of the extension and quality of the nanothread produced in the reaction of pure TS and mixed TS-TA crystals is provided by high resolution transmission electron microscopy (HRTEM). In Figure 11, we report some selected TEM micrographs

collected on the product obtained by the reaction of TS performed at 373 K and 23.3 GPa. The fragments analyzed have been obtained by grinding in small pieces the samples recovered from the different experiments and the thinner ones have been selected to maximize the transmission. As already observed in other cases and in agreement with the only partial chemical transformation of the pristine crystal, we have found large areas dominated by the presence of amorphous hydrogenated carbon (S3) and sample portions showing perfectly parallel features located to an average distance of 1.16 nm therefore in perfect agreement with the (100) diffraction peak measurd by XRD (Figure 11). These ordered regions extend for tens of nanometers. The presence of two product typologies is reasonable in view of the competing mechanisms which characterize these reactions. Moreover, the presence of amorphous regions could also be ascribed to the not yet clear interactions between nanothreads and electron beam. In the present experiment we have used a JEOL ARM200F, operating at an accelerating voltage of 60kV, to avoid the knock-on damage. It has been shown that at this voltage, well below the critical voltage of 80kV,[52] the knock-on damage in graphene is practically zero. However, there is a lack of information in literature about the electron beam interactions involved in the present system. As a matter of fact, even at low voltage the periodicity observable in Figure 11 disappeared after some minute of exposure, indicating a possible amorphization induced by the electron beam. This latter process could also explain the missed observation of the graphite diffraction peak in XRD experiments, in spite of sampling almost the entire sample, and the indication gained by the kinetic analysis of a high selectivity of the reaction (see Figure 5 and relative discussion).

As a final step of our analysis we optimized the structure and computed, using density functional theory (DFT), the energy and the IR spectra of nanothread composed by six molecular units. Among the four polymeric structures identified as the most probable, tube (3,0), polymer I, polytwistane and zipper,[25,53] we can rule out the last two because they are incompatible with the formation of double nanothreads as extensively discussed in the azobenzene case.[32] The Gibbs energy obtained for TS and TS-TA oligomers (S4)

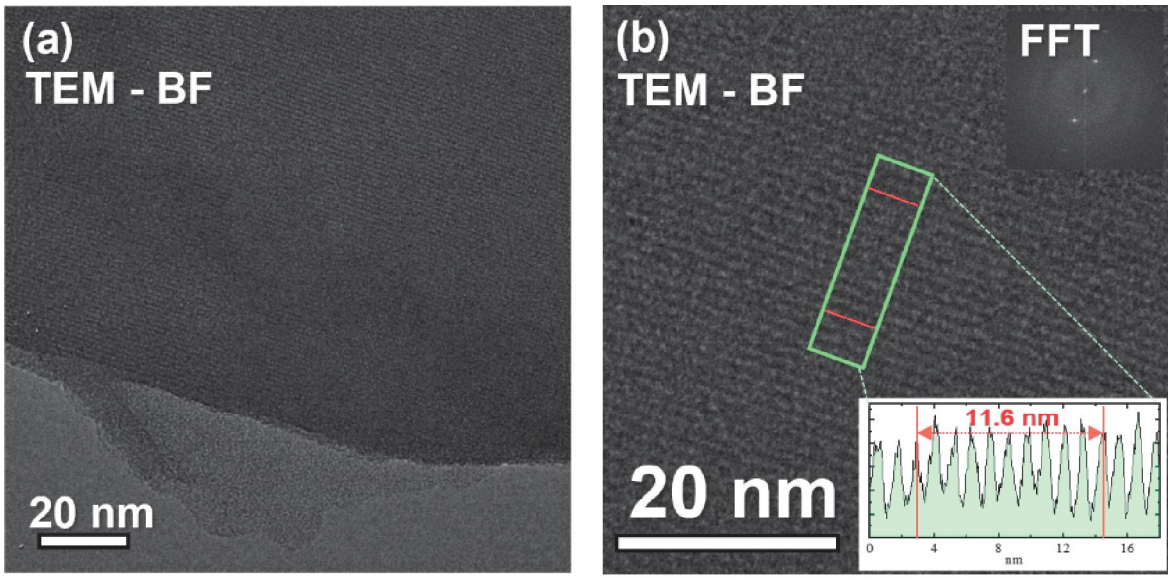

Figure 11: (a) Bright-field TEM micrograph acquired on the samples recovered by the reaction of pure TS performed at 373 K and 23.3 GPa and (b) high-resolution image inside this region. TEM analysis has been performed using an accelerating voltage of 60 kV, to avoid the knock-on damage. Ordered regions with plane spacing compatible with nanothreads and XRD results are clearly visible. The insets in (b) report the line profile obtained along the green box emphasizing a spacing of 1.16 nm, and the FFT which evidences this periodicity.

after subtracting the electronic contribution and that, of vibrational nature, related to the different number of hydrogen atoms required to saturate the chain terminations (six more H in the tube (3,0) with respect to the polymer I), is lower for the polymer I structure both for TS (0.58 eV) and TS-TA 1:1 oligomers (2.54 eV). Remarkably, in both oligomers with the tube (3,0) structure the azo and ethylenic groups linking the threads are polymerized along the thread direction driven by the bonding geometry of the carbon atom of the thread to which the linker group is connected. This occurrence determines relevant differences in the computed spectra of the tube (3,0) and polymer I oligomers consisting in a relevant intensification of the region between 1000 and 1400 cm^{-1} in the tube (3,0) structure, whereas the strong bands around 800 cm^{-1}, present in the computed spectra of polymer I and assigned to bending modes involving the hydrogen atoms bound to the ethylenic groups, consistently disappear. As shown in the Supplementary materials the comparison between the computed IR spectra and those of recovered nanothreads from the experiment sharply indicate the

polymer I as preferred structure.

The present results unambiguously outline the common behavior that TA, TS and TS-TA mixed crystals exhibit as far as concerns the structural evolution with pressure, the instability thresholds and the reaction mechanism. Pressures in excess of 20 GPa are necessary to induce the chemical transformation of 15-30 % of the monomer with appreciable rate (2-3 days). Kinetic data acquired during the transformation of the mixed TS-TA crystals attest for a high selectivity of the process. The resulting saturated carbon nanothread is stable in time at ambient conditions likely adopting, on the basis of the comparison between the computed IR spectra of short oligomers and those of the recovered materials, the polymer I structure. The reaction is anticipated, as reported in the case of azobenene,[33] by a sluggish phase transition observed both in TS and in TS-TA mixed crystals between 7 and 10 GPa when no hydrostatic pressure transmitting medium is employed. The new phase is characterized by a monoclinic angle close to 120° and a consistent reduction of the unit cell due to the strong contraction occurring along the b axis. A further compression of the new phase produces a marked anisotropic cell contraction along the b axis, a feature particularly evident in the mixed crystal where both the volume and the b parameter undergo to a 20% reduction between 9 and 16 GPa. Despite the pressure of the phase transition is much lower (about 10 GPa) of the reaction onset, which is accurately identified by IR absorption spectroscopy (see Figure 2), is unquestionable that the corresponding changes are strictly related to the reaction since the b axis indeed coincides with the direction along which the nanothreads develop. This phase transition, firstly reported in TA, was suggested to be a kind of prereactive stage where the equivalent molecules aligned along the b axis form stacks of nearly parallel molecules interacting through the π densities.[33] A quantification of the entire process requires single crystal studies compressed in hydrostatic pressure transmitting media like helium or neon or, alternatively, can be indirectly proved by the remarkable change in the electronic properties that such interaction likely entails.[54]

As expected, according to the isomorphism characterizing the pseudo-stilbene crystals,

the nanothreads obtained from TS and TS-TA mixed crystals arrange in a 2D crystal lattice with the same packing reported in the azobenzene case.[32] In that case the lattice parameters of the 2D monoclinic cell were $a = 6.46$ Å; $c = 13.05$ Å and $\beta = 120°$, whereas here we found for TS: $a = 6.67(22)$ Å and $c = 12.87(35)$ Å; whereas for TS-TA mixed crystals: $a = 6.55(5)$ Å and $c = 13.14(10)$ Å, with $\beta = 120°$ in both cases. The largest variability of the lattice parameters values in the TS case is only due to the largest number of samples investigated. Thermal annealing of the recovered carbon nanothread is accompanied by a limited ($\leq$5%) structural relaxation of the 2D arrangement whereas no effects are detectable in the thread structure. The high resolution TEM images confirm the formation of large areas, extending also several tens of nanometers, characterized by regular stripes in the product obtained by TS. In this case it was possible to identify the in-plane separation between the threads of 1.16 nm in excellent agreement with the data from XRD. Interestingly, in spite of XRD provides the same information for all the samples, we were not able to identify in the samples recovered from the reaction in the TS-TA mixed crystals any region where the striped pattern characterizing the nanothreads was visible in the TEM images. The reason can be related to the reduced accessible portion of the sample, only the thinner fragments can be studied and to the micro probing intrinsically characterizing the technique, or by a lower damage threshold of this material.

In conclusion, with this work we have demonstrated the possibility of synthesizing double-core carbon nanothreads from the most representative molecules of the pseudo-stilbenes class both from pure and mixed crystals. In all the cases azo and ethylene groups linking the two threads are preserved during the reaction, an impressive achievement in view of designing new materials where these groups can be possibly employed for further functionalization and can define targeted electronic properties. The extent of this result is further highlighted by the ease in the obtainment of mixed crystals of the desired relative concentration exploiting the isomorphism of all the pseudo-stilbenes. In addition, the use of starting molecules where substituents are present in the phenyl rings may open the way to selective functionalization

of the thread itself. The large number of the industrial and biomedical application of nanodiamonds helps to get an idea of the potential of this new material. In fact, besides exhibiting similar enhanced mechanical and thermal properties, the possibility to produce bundles of micron size open the way to their use as real fibers where, as in the case of the double-core nanothreads reported here, the threads represent an efficient protective sheath of the cromophores introduced in the desired concentration by adjusting the starting composition of the crystal.

Methods

Crystalline TS from Sigma-Aldrich (purity $> 99\%$) was used without any further treatment. TS-TA mixed crystal were prepared by dissolving in acetone the two crystalline powders (TA from Sigma-Aldrich purity $> 99\%$) in the desired ratio. The saturated solution was filtered and then slowly (3-4 days) evaporated until a single light red crystal, having a size of several millimeters, formed. All the samples were produced by milling fragments of this crystal and the powder obtained was loaded without any compression medium into a membrane diamond anvil cell (MDAC) equipped with IIas type diamonds (Almax-Easylab) together with a ruby chip for pressure calibration by the ruby fluorescence method. [55] Samples were laterally contained by stainless steel gaskets drilled to have an initial sample diameter of 150 μm and a thickness of about 50 μm. High-temperature was obtained by resistive heating, the sample temperature was measured with a K-type thermocouple placed close to the diamonds with a 0.1 K accuracy.

Angle-dispersive synchrotron X-ray diffraction measurements were performed on the recovered products at the Xpress beamline at the Elettra italian synchrotron with a beam energy of 25.0 keV, a focal spot diameter of about 80 μm (FWHM) and an image plate detector (MAR345). In-house X-ray diffraction measurements were performed with a custom made, laboratory diffractometer, equipped with a focused Xenocs-GeniX Mo small spot

microsource with a wavelength of 0.7107 Å and a beam diameter on the focal plane of 150 μm. A PI-SCX 4300 CCD was employed as detector.

Fourier transform infrared absorption spectra were recorded using a Bruker-IFS 120 HR spectrometer suitably modified for experiments in diamond anvil cell, with an instrumental resolution set to 1 cm^{-1}.[56] The ruby fluorescence was excited using few mW of a 532 nm laser line from a doubled Nd:YAG laser source.

Transmission electron microscopy (TEM) investigation was performed with a JEOL ARM200F Cs-corrected microscope, equipped with a cold-field emission gun having an energy spread of 0.3 eV and operating at 60 keV. In conventional TEM (CTEM) mode, micrographs have been acquired in bright field (BF), while in STEM mode imaging has been also performed in Z-contrast mode using a high-angle annular dark field (HAADF) detector, with a probe size of 1.0 Å. The recovered material was mechanically removed from the gasket with a needle and placed directly onto the surface of a standard TEM lacey carbon film, covering a 300-mesh copper grid.

Quantum chemistry calculations were performed using the Gaussian16 software[57] to obtain optimized structures and vibrational frequencies for the isolated fully sp^3 nanothread fragments composed by six molecular units having the polymer I and the tube (3,0) structures. The calculation were performed using the density functional theory (DFT), adopting the Becke's three-parameter hybrid exchange functional and Lee–Yang–Parr correlation functional (B3LYP)[58,59] using the 6-311G(d,p) basis set. No imaginary vibrational frequencies were obtained indicating that the optimized vacuum geometries were at the minimum of the potential surface.

Conflicts of interest

There are no conflicts to declare.

Acknowledgements

We thank the European Laboratory for Nonlinear Spectroscopy (LENS) for hosting the research, the Deep Carbon Observatory and the "Fondazione CR Firenze" for strong support. The research has been supported by the following grants: Extreme Physics and Chemistry of Carbon: Forms, Transformations, and Movements in Planetary Interiors funded by the Alfred P. Sloan Foundation; Fondazione Cassa di Risparmio di Firenze under the project "Utilizzo dell'anisotropia strutturale nella sintesi di nanofili di carbonio diamond-like ad alta pressione". The TEM analyses were performed at Beyond-Nano laboratory of the CNR-IMM, which is supported by the Italian Ministry of Education and Research (MIUR) under the "Beyond-Nano" project (PON a3_00363). This project has received funding from the European Union's Horizon 2020 research and innovation programme under grant agreement No 823717 – ESTEEM3. We also thank the Elettra italian syncrhotron for hosting our experiment under the proposal number 20200230.

References

(1) *Carbon Nanomaterials: Modeling, Design, and Applications* K. Zhou Ed., CRC Press, Boca Raton, Florida, 2nd Ed., 2019.

(2) *Carbon Nanomaterials*, Y. Gogotsi, V. Presser Eds., CRC Press, Boca Raton, Florida, 2nd Ed., 2017.

(3) *Carbon Nanomaterials for Advanced Energy Systems*, W. Lu, J.-B. Baek, L. Da Eds., John Wiley & Sons, Inc., Hoboken, New Jersey, 2015.

(4) A. C. Ferrari et al. Science and Technology Roadmap for Graphene, related Two-Dimensional Crystals, and Hybrid Systems. *Nanoscale*, 2015, **7**, 4587-5062.

(5) J. L. Blackburn, A. J. Ferguson, C. Cho and J. C. Grunlan, Carbon-Nanotube-Based Thermoelectric Materials and Devices. *Adv. Mater.*, 2018, **30**, 1704386.

(6) Lv, T.; Liu, M.; Zhu, D.; Gan, L.; Chen, T. Nanocarbon-Based Materials for Flexible All-Solid-State Supercapacitors. *Adv. Mater.* **2018**, *30*, 1705489.

(7) V. N. Mochalin, O. Shenderova, D. Ho and Y. Gogotsi, The Properties and Applications of Nanodiamonds. *Nature Nanotechnol.*, 2011, **7**, 11-23.

(8) Roman, R. E.; Kwan, K.; Cranford, S. W. Mechanical Properties and Defect Sensitivity of Diamond Nanothreads. *Nano Lett.* **2015**, *15*, 1585-1590.

(9) Stojkovic, D.; Zhang, P.; Crespi, V. H. Smallest Nanotube: Breaking the Symmetry of sp^3 Bonds in Tubular Geometries. *Phys. Rev. Lett.* **2001**, *87*, 125502.

(10) Wen, X.-D.; Hoffmann, R.; Ashcroft, N. W. Benzene under High Pressure: a Story of Molecular Crystals Transforming to Saturated Networks, with a Possible Intermediate Metallic Phase. *J. Am. Chem. Soc.* **2011**, *133*, 9023-9035.

(11) Barua, S. R.; Quanz, H.; Olbrich, M.; Schreiner, P. R.; Trauner, D.; Allen, W. D. Polytwistane. *Chem. - Eur. J.* **2014**, *20*, 1638-1645.

(12) Fitzgibbons, T. C.; Guthrie, M.; Xu, E. S.; Crespi, V. H.; Davidowski, S. K.; Cody, G. D.; Alem, N.; Badding, J. V. Benzene-Derived Carbon Nanothreads. *Nature Mater.* **2015**, *14*, 43-47.

(13) Zhan, H.; Zhang, G.; Bell, J. M.; Tan, V. B. C.; Gu, Y. High Density Mechanical Energy Storage with Carbon Nanothread Bundle. *Nature Comm.* **2020**, *11*, 1905.

(14) Zhan, H.; Zhang, G.; Zhuang, G.; Timon, R.; Gu, Y. Low Interfacial Thermal Resistance between Crossed Ultra-Thin Carbon Nanothreads. *Carbon* **2020**, *165*, 216-224.

(15) Li, X.; Wang, T.; Duan, P.; Baldini, M.; Huang, H.-T.; Chen, B.; Juhl, S. J.; Koeplinger, D.; Crespi, V. H.; Schmidt-Rohr, K.; Hoffmann, R.; Alem, N.; Guthrie, M.; Zhang, X.; Badding, J. V. Carbon Nitride Nanothread Crystals Derived from Pyridine. *J. Am. Chem. Soc.* **2018**, *140*, 4969-4972.

(16) Fanetti, S.; Santoro, M.; Alabarse, F.; Berretti, E.; Bini, R. Modulating the H-Bond Strength by Varying the Temperature for the High Pressure Synthesis of Nitrogen Rich Carbon Nanothreads. *Nanoscale* **2020**, *12*, 5233-5242.

(17) Nobrega, M. M.; Teixeira-Neto, E.; Cairns, A. B.; Temperini, M. L. A.; Bini, R. One-Dimensional Diamondoid Polyaniline-like Nanothreads from Compressed Crystal Aniline. *Chem. Sci.* **2018**, *9*, 254-260.

(18) Biswas, A.; Ward, M. D.; Wang, T.; Zhu, L.; Huang, H.-T.; Badding, J. V.; Crespi, V. H.; Strobel, T. A. Evidence for Orientational Order in Nanothreads Derived from Thiophene. *J. Phys. Chem. Lett.* **2019**, *10*, 7164–7171.

(19) Huss, S.; Wu, S.; Chen, B.; Wang, T.; Gerthoffer, M. C.; Ryan, D. J.; Smith, S. E.; Crespi, V. H.; Badding, J. V.; Elacqua, E. Scalable Synthesis of Crystalline One-

Dimensional Carbon Nanothreads through Modest-Pressure Polymerization of Furan *ACS Nano* **2021**, *15*, 4134-4143.

(20) Ward, M. D.; Tang, W. S.; Zhu, L.; Popov, D.; Cody, G. D.; Strobel, T. A. Controlled Single-Crystalline Polymerization of $C_{10}H_8 \cdot C_{10}F_8$ under Pressure. *Macromolecules* **2019**, *52*, 7557-7563.

(21) Friedrich, A.; Collings, I. E.; Dziubek, K.; Fanetti, S.; Radacki, K.; Ruiz-Fuertes, J.; Pellicer-Porres, J.; Hanfland, M.; Sieh, D.; Bini, R.; Clark, S. J.; Marder, T. B. Pressure-Induced Polymerization of Polycyclic Arene-Perfluoroarene co-Crystals: Single Crystal X-Ray Diffraction Studies, Reaction Kinetics, and Design of Columnar Hydrofluorocarbons. *J. Am. Chem. Soc.* **2020**, https://dx.doi.org/10.1021/jacs.0c09021.

(22) H.-T. Huang, L. Zhu, M. D. Ward, T. Wang, B. Chen, B. L. Chaloux, Q. Wang, A. Biswas, J. L. Gray, B. Kuei, G. D. Cody, A. Epshteyn, V. H. Crespi, J. V. Badding, T. A. Strobel Nanoarchitecture through Strained Molecules: Cubane-Derived Scaffolds and the Smallest Carbon Nanothreads. *J. Am. Chem. Soc.* **2020**, *142*, 17944-17955.

(23) Demingos, P. G.; Muniz, A. R. Carbon Nanothreads from Polycyclic Aromatic Hydrocarbon Molecules. *Carbon* **2018**, *140*, 644-652.

(24) Silveira, J. F. R. V.; Muniz, A. R. Functionalized Diamond Nanothreads from Benzene Derivatives. *Phys. Chem. Chem. Phys.* **2017**, *19*, 7132-7137.

(25) Chen, B.; Hoffmann, R.; Ashcroft, N. W.; Badding, J.; Xu, E. S.; Crespi, V. Linearly Polymerized Benzene Arrays As Intermediates, Tracing Pathways to Carbon Nanothreads. *J. Am. Chem. Soc.* **2015**, *137*, 14373-14386

(26) Li, X.; Baldini, M.; Wang, T.; Chen, B.; Xu, E.-s.; Vermilyea, B.; Crespi, V. H.; Hoffmann, R.; Molaison, J. J.; Tulk, C. A.; Guthrie, M.; Sinogeikin, S.; Badding, J. V. Mechanochemical Synthesis of Carbon Nanothread Single Crystals. *J. Am. Chem. Soc.* **2017**, *139*, 16343-16349.

(27) Fanetti, S.; Nobrega, M. M.; Teixeira-Neto, E.; Temperini, M. L. A.; Bini, R. Effect of Structural Anisotropy in High-Pressure Reaction of Aniline. *J. Phys. Chem. C* **2018**, *122*, 29158-29164.

(28) Duan, P.; Li, X.; Wang, T.; Chen, B.; Juhl, S. J.; Koeplinger, D.; Crespi, V. H.; Badding, J. V.; Schmidt-Rohr, K. The Chemical Structure of Carbon Nanothreads Analyzed by Advanced Solid-State NMR. *J. Am. Chem. Soc.* **2018**, *140*, 7658-7666.

(29) Juhl, S. J.; Wang, T.; Vermilyea, B.; Li, X.; Crespi, V. H.; Badding, J. V.; Alem, N. Local Structure and Bonding of Carbon Nanothreads Probed by High-Resolution Transmission Electron Microscopy. *J. Am. Chem. Soc.* **2019**, *141*, 6937-6945.

(30) Zhan, H.; Zhang, G.; Tan, V. B. C.; Cheng, Y.; Bell, J. M.; Zhang, Y.-W.; Gu, Y. From Brittle to Ductile: a Structure Dependent Ductility of Diamond Nanothread. *Nanoscale* **2016**, *8*, 11177-11184.

(31) Demingos, P. G.; Muniz, A. R. Electronic and Mechanical Properties of Partially Saturated Carbon and Carbon Nitride Nanothreads. *J. Phys. Chem. C* **2019**, *123*, 3886-3891.

(32) Romi, S.; Fanetti, S.; Alabarse, F.; Mio, A. M.; Bini, R. Synthesis od Double Core Chromophore Functionalized Nanothreads by Compressing Azobenzene in a Diamond Anvil Cell *Chem. Sci.* **2021**, DOI: 10.1039/D0SC06968J.

(33) Romi, S.; Fanetti, S.; Alabarse, F.; Bini, R. Structure-Reactivity Relationship in the High-Pressure Formation of Double Core Carbon Nanothreads from Azobenzene Crystal *J. Phys. Chem. C* **2021**, *125*, 17174-17182.

(34) Wagner-Wysiecka, E.; Łukasik, N.; Biernat, J. F.; Luboch, E. Azo Group(s) in Selected Macrocyclic Compounds. *J. Incl. Phenom. Macrocycl. Chem.* **2018**, *90*, 189–257.

(35) Bléger, D.; Hecht, S. Visible-Light-Activated Molecular Switches. *Angew.Chem.Int. Ed.* **2015**, *54*, 11338 –11349.

(36) Crespi, S.; Simeth, N. A.; König, B. Heteroaryl Azo Dyes as Molecular Photoswitches. *Nature Rev. Chem.* **2019**, *3*, 133–146.

(37) Dong, M.; Babalhavaeji, A.; Samanta, S.; Beharry, A. A.; Woolley, G. A. Red-Shifting Azobenzene Photoswitches for in Vivo Use. *Acc. Chem. Res.* **2016**, *7*, 11090.

(38) M. Döbbelin et al. Light-Enhanced Liquid-Phase Exfoliation and Current Photoswitching in Graphene-Azobenzene Composites *Nature Commun.* **2015**, *48*, 2662–2670.

(39) Bouwstra, J. A.; Schouten, A.; Kroon, J. Structural Studies of the System Trans-Azobenzene/Trans-Stilbene. I. A Reinvestigation of the Disorder in the Crystal Structure of Trans-Azobenzene, $C_{12}H_{10}N_2$. *J. Acta Crystallogr., Sect. C: Cryst. Struct. Commun.* **1983**, *C39*, 1121-1123.

(40) Bouwstra, J. A.; Schouten, A.; Kroon, J.; Helmholdt, R. B. Structural studies of the system trans-stilbene/trans-azobenzene. II. A Reinvestigation of the Disorder in the Crystal Structure of trans-stilbene, $C_{14}H_{12}$ *J. Acta Crystallogr., Sect. C: Cryst. Struct. Commun.* **1984**, *C40*, 428-431.

(41) Bouwstra, J. A.; Schouten, A.; Kroon, J.; Helmholdt, R. B. Structural studies of the system trans-stilbene/trans-azobenzene. III. The structures of three mixed crystals of trans-azobenzene/trans-stilbene; determinations by X-ray and neutron diffraction *J. Acta Crystallogr., Sect. C: Cryst. Struct. Commun.* **1985**, *C41*, 420-426.

(42) Harada, J.; Ogawa, K. X-ray Diffraction Analysis of Nonequilibrium States in Crystals: Observation of an Unstable Conformer in Flash-Cooled Crystals. *J. Am. Chem. Soc.* **2004**, *126*, 3539-3544.

(43) Meić, Z.; Güsten, H. Vibrational studies of Trans-Stilbenes—I. Infrared and Raman Spectra of Trans-Stilbene and Deuterated Trans-Stilbenes. *Spectrochim. Acta A* **1978**, *34*, 101–111.

(44) Avrami, M. Kinetics of Phase Change. I General Theory. *J. Chem. Phys.* **1939**, *7*, 1103-1112.

(45) Avrami, M. Kinetics of Phase Change. II Transformation-Time Relations for Random Distribution of Nuclei. *J. Chem. Phys.* **1940**, *8*, 212-224.

(46) Avrami, M. Granulation, Phase Change, and Microstructure Kinetics of Phase Change. III. *J. Chem. Phys.* **1941**, *9*, 177-184.

(47) Hulbert, S. F. Models for Solid-State Reactions in Powdered Compacts: A Review. *J. Br. Ceram. Soc.* **1969**, *6*, 11-20.

(48) Romi, S.; Fanetti, S.; Bini, R. Accessing the Activation Mechanisms of Ethylene Photo-Polymerization under Pressure by Transient Infrared Absorption Spectroscopy *J. Phys. Chem.* **2020**, *124*, 8149-8157.

(49) Ciabini, L.; Santoro, M.; Bini, R.; Schettino, V. High Pressure Reactivity of Solid Benzene Probed by Infrared Spectroscopy. *J. Chem. Phys.* **2002**, *116*, 2928-2935.

(50) Citroni, M.; Fanetti, S.; Bazzicalupi, C.; Dziubek, K.; Pagliai, M.; Nobrega, M. M.; Mezouar, M.; Bini, R. Structural and Electronic Competing Mechanisms in the Formation of Amorphous Carbon Nitride by Compressing s-Triazine. *J. Phys. Chem. C* **2015**, *119*, 28560-28569.

(51) Lin-Vien, D.; Colthup, N. B.; Fateley, W. G.; Grasselli, J. G. *Handbook of Infrared and Raman Characteristic Frequencies of Organic Molecules*; Academic Press: San Diego, CA, 1991.

(52) Meyer, J. C.; Eder, F.; Kurasch, S.; Skakalova, V.; Kotakoski, J.; Park, H. J.; Roth, S.; Chuvilin, A.; Eyhusen, S.; Benner, G.; Krasheninnikov, A. V.; Kaiser, U. Accurate Measurement of Electron Beam Induced Displacement Cross Sections for Single-Layer Graphene *Phys. Rev. Lett.* **2012** , *108*, 196102.

(53) Chen, B.; Wang, T.; Crespi, V. H.; Li, X.; Badding, J.; Hoffmann, R. All the Ways To Have Substituted Nanothreads. *J. Chem. Theory Comput.* **2018**, *14*, 1131-1140.

(54) Citroni, M.; Bini, R.; Foggi, P.; Schettino, V. Role of excited electronic states in the high-pressure amorphization of benzene. *Proc. Natl. Ac. Sci.* **2008**, *105*, 7658–7663.

(55) Mao, H. K.; Bell, P. M.; Shaner, J. V.; Steinberg, D. J. Specific Volume Measurements of Cu, Mo, Pd, and Ag and Calibration of the Ruby R1 Fluorescence Pressure Gauge from 0.06 to 1 Mbar. *J. Appl. Phys.* **1978**, *49*, 3276.

(56) Bini, R.; Ballerini, R.; Pratesi, G.; Jodl, H. J. Experimental Setup for Fourier Transform Infrared Spectroscopy Studies in Condensed Matter at High Pressure and Low Temperatures. *Rev. Sci. Instrum.* **1997**, *68*, 3154-3160.

(57) Frisch, M. J.; et al. Gaussian 16, Revision B.01, Gaussian, Inc., Wallingford CT, 2016.

(58) Becke, A. D. A New Mixing of Hartree–Fock and Local Density-Functional Theories J. Chem. Phys., 1993, 98, 1372-1377.

(59) Lee, C.; Yang, W.; Parr, R. G. Development of the Colle-Salvetti Correlation-Energy Formula into a Functional of the Electron Density Phys. Rev. B: Condens. Matter Mater. Phys., 1988, 37, 785–789.

Graphical TOC Entry